Fine structure of α decay from the variational principle

M. Mirea*

Horia Hulubei National Institute for Physics and Nuclear Engineering, P.O. Box MG-6, 077125 Bucharest-Magurele, Romania;
Faculty of Physics, University of Bucharest, Atomistilor Street 405, Bucharest-Magurele, Romania;
and Academy of Romanian Scientists, Splaiul Independentei 54, 050094 Bucharest, Romania

(Received 5 September 2017; revised manuscript received 24 October 2017; published 14 December 2017)

Starting from the variational principle, the time-dependent pairing equations are generalized by including the Landau-Zener effect and the Coriolis coupling. A system of microscopic equations of motion for configuration mixing is deduced, allowing the determination of quantities that have the same meaning as the preformation factors of the α particle. These equations are solved in order to reproduce the hindrance factors of the α decay of an odd-A mass nucleus. The α decay of ^{211}Po is treated as a superasymmetric fission process, by following the rearrangement of the nuclear orbitals from the parent ground state up to the scission configuration. The probabilities of finding the excited states of the daughter at scission are obtained from the microscopic equations of motion. The intensities of the transitions to the excited states of the daughter were evaluated theoretically. The experimental data were compared with the theoretical findings. A very good agreement was obtained. A mean value of the tunneling velocity of about 2×10^4 fm/fs was extracted.

DOI: 10.1103/PhysRevC.96.064607

I. INTRODUCTION

A new system of microscopic equations of motion for seniority-1 configuration mixings, that allows at the same time the deduction of the time-dependent pairing equations, is obtained from the variational principle. The time-dependent pairing equations, formally similar to the time-dependent Hartree-Fock-Bogoliubov equations, are able to supply an estimation of the dissipated energy. The Coriolis coupling and the Landau-Zener effect are mechanisms introduced in this new system of differential equations, allowing single particle excitations, i.e., a change of the configurations. The formalism is used to evaluate the branching ratio in the α-decay fine structure of ^{211}Po.

α decay is the spontaneous emission of a He nucleus. In the phenomenological description, a preformed α particle penetrates an external barrier and attains an energy close to the Q value of the reaction. The microscopic part in the description of this process concerns the modality in which the particle is born on the surface of the daughter nucleus [1–4]. Usually, the preformation factor of the α particle is calculated as an overlap between the initial configuration of the parent ground state and the final configuration of the two nuclei close to scission [5]. The fine structure of the α emission reveals modifications of the emission probabilities for different excited states of the daughter nucleus. This phenomenon was evidenced by Rosenblum in 1929 by measuring the ranges of α particles in the air [6,7]. The kinetic energy of the α particle has several values that can be associated with a specific excitation of the daughter nucleus. Microscopically, a phonon operator acting on the daughter nucleus ground state may describe such an excited state [8]. In the case of the α radioactivity of ^{211}Po, each final state is characterized by a single particle excitation that can be associated with a specific seniority-1 configuration. In order to investigate the the fine structure phenomenon, it is possible to consider that the total wave function of the decaying system is a superposition of core-angular harmonic [9] functions; that is, of combinations between an interval wave function and an external one, connected smoothly in the nuclear surface region of the daughter nucleus. By using the orthogonality property of the core-angular harmonics and projecting them on different channels, a coupled channel description of the α-decay fine structure can be obtained. Calculations based on this formalism were initiated in Ref. [10] and generalized to take into account vibrational [11] and rotational [12] excitations.

In these enumerated theories, the α particle is always preformed on the nuclear surface, the dynamics of its formation being unclear. But, the α particle cannot appear suddenly on the surface of the daughter, even in the case when the α particle preexists in the parent nucleus. As stated by Hill and Wheeler in a seminal paper published in 1953 [13], due to the extreme saturation of nuclear matter, the states of the nucleons mainly depend on the boundaries of the many-body potential. If the α particle preexists in the parent nucleus and it is moving to the external region, implicitly the nuclear shape of the whole system is modified. That is, all the nucleons states are perturbed during the α-decay process. Therefore, a simple picture consisting of an overlap between an unperturbed initial state and a final configuration should be not sufficient to take into account the whole complexity of the process.

In my formalism, one follows the rearrangement of the microscopic states during the emission of an α particle, beginning from the parent ground state and reaching the scission. The emission of the α particle is simulated by modifying the boundaries of the many body potential as realized in fission-like theories. At scission, two mean field potentials are obtained: one for the daughter nucleus and another for the α-particle. The probabilities of obtaining different single-particle excitations are given by the solutions of a system of equations of motion for superfluid systems.

*mirea@ifin.nipne.ro

In the next section, this system of equations is deduced. It should be mentioned that a first attempt to explain dynamically the α-decay fine structure was realized in Ref. [14] with a system of equations of motion in which the pairing field was neglected. The calculations performed for the α decay of ^{211}Po are presented in Sec. III. The last section is dedicated to conclusions.

II. TIME-DEPENDENT EQUATIONS OF MOTION

During the evolution of a many-body system, two dynamical promotion effects arise, leading to single-particle excitations: the Landau-Zener effect and the Coriolis one [15,16]. Both effects are included in the new system of equations of motion deduced in the following. The microscopic equations of motion for the configuration mixing are obtained from the variational principle. These equations should give the probabilities of finding the nuclear system in different seniority-1 configurations during the evolution in time of the nuclear system and the dynamical values of the BCS amplitudes. The energy functional is

$$\delta L = \delta\langle\varphi_{IM}|H + H_R - i\hbar\frac{\partial}{\partial t} + H' - \lambda\hat{N}|\varphi_{IM}\rangle, \quad (1)$$

where the many-body state is considered as a superposition of products between seniority-1 Bogoliubov wave functions and rotation functions:

$$|\varphi_{IM}\rangle = \sum_{\Omega,m} c_{\Omega,m}|\varphi_{IM\Omega m}\rangle = \sum_{\Omega,m} c_{\Omega,m} b^{+}_{I,M,\Omega,m} \prod_{(\Omega_1,m_1)\neq(\Omega,m)} \times \left(u_{\Omega_1,m_1(\Omega,m)} + v_{\Omega_1,m_1(\Omega,m)} a^{+}_{\Omega_1,m_1} a^{+}_{\bar{\Omega}_1,m_1}\right)|0\rangle. \quad (2)$$

Here, $a^{+}_{\Omega,m}$ and $a_{\Omega,m}$ are the single-particle creation and annihilation operators, and $c_{\Omega,m}$ are the amplitudes of the seniority-1 configurations. Therefore, the value of $|c_{\Omega,m}|^2$ gives the probabilities of finding the configurations with an unpaired nucleon located on the single-particle level labeled by the quantum numbers (Ω,m). In my notations, Ω denotes the intrinsic spin projection on the axis of symmetry, and m is a number that identifies the single-particle state located in the same Ω level's subspace. The variables $u_{\Omega_1,m_1(\Omega,m)}$ and $v_{\Omega_1,m_1(\Omega,m)}$ denote the BCS vacancy and occupation amplitudes for the single-particle states (Ω_1,m_1) in the seniority-1 configuration in which the the single-particle state (Ω,m) is occupied by an unpaired nucleon. Because only the relative phases between these amplitudes matter, the vacancy amplitude will be considered a real quantity and the occupation amplitude is taken as a complex variable. In the expression (2), the blocking effect is included; that is, the variations of the BCS amplitudes in accordance with the seniority-1 configurations are taken into consideration.

I used the following notation for the operator $b^{+}_{I,M,\Omega,m}$ that creates a rotating state:

$$b^{+}_{I,M,\Omega,m}|0\rangle = \left(\frac{2I+1}{8\pi^2}\right)^{1/2}\left(\frac{\Omega}{|\Omega|}\right)^{I+\Omega}\mathcal{D}^{I}_{M\Omega}(\omega)a^{+}_{\Omega,m}|0\rangle. \quad (3)$$

Here, $\mathcal{D}^{I}_{M\Omega}(\omega)$ denotes the rotation function with

$$\bar{\Omega} = -\Omega, \quad (4)$$

Ω being positive and the bar over a symbol meaning the time reversed state in a pair. The rotation functions exhibit the following relevant properties:

$$I_{\pm}\mathcal{D}^{I}_{M\Omega}(\omega) = [(I\pm\Omega)(I\mp\Omega+1)]^{1/2}\mathcal{D}^{I}_{M\Omega\pm1}(\omega), \quad (5)$$

where the ladder operators are introduced through the usual definition $I_{\pm} = I_x \pm iI_y$ in terms of the angular momenta components.

In the energy functional (1) several terms are included as explained below. The many-body Hamiltonian with pairing residual interaction is

$$H = \sum_{\Omega,m}\epsilon_{\Omega,m}(a^{+}_{\Omega,m}a_{\Omega,m} + a^{+}_{\bar{\Omega},m}a_{\bar{\Omega},m}) - G\sum_{(\Omega,m)(\Omega_1,m_1)} a^{+}_{\Omega,m}a^{+}_{\bar{\Omega},m}a_{\Omega_1,m_1}a_{\bar{\Omega}_1,m_1}, \quad (6)$$

where $\epsilon_{\Omega,m}$ are single-particle energies and G is a constant pairing interaction.

The axial symmetric rotor energy [17] is

$$H_R = \frac{\hbar^2}{2J}\left(I^2 - j_z^2\right) + \frac{\hbar^2}{2J}\left(j_x^2 + j_y^2\right) - \frac{\hbar^2}{2J}(j_+I_- + j_-I_+), \quad (7)$$

where J is the total momentum of inertia, $I = (I_x, I_y, I_z)$ is the total angular momentum, and $j = (j_x, j_y, j_z)$ is the intrinsic angular momentum of a particle. The first term in the right-hand side of the expression (7) is a constant of motion. The second term $(\hbar^2/2J)(j_x^2 + j_y^2)$ is called the recoil term and acts only on the intrinsic wave functions. Therefore, as proposed in Ref. [17], it is considered to be absorbed in the Hamiltonian responsible for the single-particle motion. This last assertion is contradicted by the conclusions given in Ref. [18], where an analysis of the influence of this term on the rotational structure was realized. It was evidenced that this term cannot be properly included in the Hamiltonian due to its dependence on the rotational parameter $\hbar^2/2J$. This behavior implies that the potential parameters should be deformation dependent. But, as mentioned in Ref. [19], the recoil term does not perturb significantly the intrinsic wave functions. For simplicity, in the following I will refer to the particle rotor model without recoil. The third term in the expression (7) represents an interaction between a particle and the rotational motion, known as the Coriolis coupling. The Coriolis coupling can shift nucleons from one single-particle level to another, allowing a change of the configuration.

A Landau-Zener term is introduced in the functional (1), to simulate an effect for the dynamical promotion of a nucleon between diabatic single-particle levels characterized by the same good quantum numbers in avoided level crossing regions [20,21]. As specified in Refs. [22,23] the interaction that allows this promotion mechanism contribution in superfluid systems

has the following form:

$$H' = \sum_{\Omega,m,m'} h_{\Omega,m,m'} \alpha^{+}_{\Omega,m(\Omega,m')} \alpha_{\Omega,m'(\Omega,m)} \times \prod_{\Omega',m''} \alpha_{\Omega',m''(\Omega,m')} a^{+}_{\Omega',m''} a_{\Omega',m''} \alpha^{+}_{\Omega',m''(\Omega,m)}, \quad (8)$$

where $h_{\Omega,m,m'}$ are the interactions between the states (Ω,m) and (Ω,m') in the avoided level crossing regions. I introduced the quasiparticle creation and annihilation operators, $\alpha^{+}_{\Omega,m(\Omega,m')} = (u_{\Omega,m(\Omega,m')} a^{+}_{\Omega,m} - v^{*}_{\Omega,m(\Omega,m')} a_{\bar{\Omega},m})$ and $\alpha_{\Omega,m'(\Omega,m)} = (u_{\Omega,m'(\Omega,m)} a_{\Omega,m'} - v_{\Omega,m'(\Omega,m)} a^{+}_{\bar{\Omega},m'})$, respectively. Due to the interaction $h_{\Omega,m,m'}$, an exchange of nucleons can be made between different single particle levels (Ω,m) and (Ω,m'). The coupling matrix element $h_{\Omega,m,m'}$ is independent of the pairing interaction G. However, the promotion probability of a nucleon in an avoided level crossing region is managed by the term H' given by Eq. (8). This term depends on the BCS vacancy or occupation amplitudes. These last quantities depend on the pairing interaction. The magnitude of the coupling matrix element $h_{\Omega,m,m'}$ can be extracted directly from the energy diagram. The maximum value of $h_{\Omega,m,m'}$ is obtained by calculating the difference of energies at the point of nearest approach between the adiabatic levels in an avoided level crossing region [24]. The product in Eq. (8) runs on all states of the selected pairing levels space, excepting the states $(\Omega,m(\Omega,m'))$ and $(\Omega,m'(\Omega,m))$. As discussed in Ref. [23], due to the interaction H', the diabatic wave function $|\varphi_{IM\Omega m}\rangle$ of the superposition (2) will be "transmitted" on the diabatic level and "reflected" on the adiabatic one after the passage of the avoided level crossing region. A dynamical pair breaking mechanism [25,26] was also described with interactions similar to that given by relation (8). Dynamical excitations in large scale collective motion are also investigated by means of quasiparticle operators in Ref. [27]. For deformed axially symmetric nuclei, the good quantum number is the spin projection Ω.

The particle number operator is written as

$$\hat{N} = \sum_{\Omega,m} (a^{+}_{\Omega,m} a_{\Omega,m} + a^{+}_{\bar{\Omega},m} a_{\bar{\Omega},m}), \quad (9)$$

and λ is the Fermi energy. The sums run over the pairing active space of single-particle levels.

The expectation value of the energy functional (1) is obtained by summing over the intermediate states given by the trial function (2):

$$\begin{aligned}
&\langle \varphi_{IM} | H + \frac{\hbar^2}{2J}\left(I^2 - j_z^2\right) - \frac{\hbar^2}{2J}(j_+ I_- + j_- I_+) - i\hbar\frac{\partial}{\partial t} + H' - \lambda N | \varphi_{IM} \rangle \\
&= \sum_{\Omega,m} |c_{\Omega,m}|^2 \Bigg\{ 2 \sum_{(\Omega',m') \neq (\Omega,m)} |v_{\Omega',m'(\Omega,m)}|^2 (\epsilon_{\Omega',m'} - \lambda) + (\epsilon_{\Omega,m} - \lambda) \\
&- G \Bigg| \sum_{(\Omega'm') \neq (\Omega,m)} u_{\Omega',m'(\Omega,m)} v_{\Omega',m'(\Omega,m)} \Bigg|^2 - G \sum_{(\Omega',m') \neq (\Omega,m)} |v_{\Omega',m'(\Omega,m)}|^4 \Bigg\} + \frac{\hbar^2}{2J} \sum_{\Omega,m} |c_{\Omega,m}|^2 [I(I+1) - \Omega^2] \\
&- \frac{\hbar^2}{2J} \Bigg\{ \sum_{\Omega} \sum_{m',m} c^{*}_{\Omega+1,m'} c_{\Omega,m} [(I-\Omega)(I+\Omega+1)]^{1/2} [u_{\Omega,m(\Omega+1,m')} u_{\Omega+1,m'(\Omega,m)} + v^{*}_{\Omega,m(\Omega+1,m')} v_{\Omega+1,m'(\Omega,m)}] \\
&\times \langle \Omega+1, m' | j_+ | \Omega, m \rangle T_{\Omega+1,m',\Omega,m} + \sum_{\Omega} \sum_{m',m} c^{*}_{\Omega-1,m'} c_{\Omega,m} [(I+\Omega)(I-\Omega+1)]^{1/2} \\
&\times [u_{\Omega,m(\Omega-1,m')} u_{\Omega-1,m'(\Omega,m)} + v^{*}_{\Omega,m(\Omega-1,m')} v_{\Omega-1,m'(\Omega,m)}] \langle \Omega-1, m' | j_- | \Omega, m \rangle T_{\Omega-1,m',\Omega,m} \Bigg\} - i\hbar \sum_{\Omega,m} |c_{\Omega,m}|^2 \\
&\times \Bigg[\sum_{(\Omega',m') \neq (\Omega,m)} \frac{1}{2} (v^{*}_{\Omega',m'(\Omega,m)} \dot{v}_{\Omega',m'(\Omega,m)} - \dot{v}^{*}_{\Omega'm'(\Omega,m)} v_{\Omega',m'(\Omega,m)}) \Bigg] - i\hbar \sum_{\Omega,m} c^{*}_{\Omega,m} \dot{c}_{\Omega,m} + \sum_{\Omega,m,m' \neq m} h_{\Omega,m',m} c^{*}_{\Omega,m'} c_{\Omega,m}. \quad (10)
\end{aligned}$$

Here, I denoted

$$|\Omega,m\rangle = a^{+}_{\Omega,m} |0\rangle \quad (11)$$

the eigenvectors characterized by the quantum numbers (Ω,m). The overlaps of the products of quasiparticles of the BCS wave functions are denoted

$$\begin{aligned}
T_{\Omega',m',\Omega,m} &= \left\langle 0 \left| \prod_{\Omega_1,m_1} \left(u_{\Omega_1,m_1(\Omega',m')} + v_{\Omega_1,m_1(\Omega',m')} a^{+}_{\Omega_1,m_1} a^{+}_{\bar{\Omega}_1,m_1}\right) \right| \prod_{\Omega_2,m_2} \left(u_{\Omega_2,m_2(\Omega,m)} + v_{\Omega_2,m_2(\Omega,m)} a^{+}_{\Omega_2,m_2} a^{+}_{\bar{\Omega}_2,m_2}\right) \right| 0 \right\rangle \\
&= \prod_{\Omega_1,m_1} \left[u_{\Omega_1,m_1(\Omega',m')} u_{\Omega_1,m_1(\Omega,m)} + v^{*}_{\Omega_1,m_1(\Omega',m')} v_{\Omega_1,m_1(\Omega,m)} \right], \quad (12)
\end{aligned}$$

where the indexes (Ω_1,m_1) run over the active pairing level space, excepting the states (Ω',m') and (Ω,m). These terms reflect the transformation of the products of the wave functions from one configuration to another one. If the blocking effect is neglected, then $T_{\Omega',m',\Omega,m}$ should be unity.

After variation, the expression (10) should supply the time-dependent evolutions of the independent variables $v_{\Omega',m'(\Omega,m)}$, $c_{\Omega,m}$ and of their complex conjugates. To obtain the time-dependent equations for configuration mixings, the expression (10) is derived with respect the independent variables c_m or c_m^*. The next equations follow:

$$
\begin{aligned}
-i\hbar\dot{c}^*_{\Omega,m} = c^*_{\Omega,m}\Bigg\{ & 2\sum_{(\Omega',m')\neq(\Omega,m)} |v_{\Omega',m'(\Omega,m)}|^2(\epsilon_{\Omega',m'}-\lambda)+(\epsilon_{\Omega,m}-\lambda) \\
& - G\Bigg|\sum_{(\Omega'm')\neq(\Omega,m)} u_{\Omega',m'(\Omega,m)}v_{\Omega',m'(\Omega,m)}\Bigg|^2 - G\sum_{(\Omega',m')\neq(\Omega,m)}|v_{\Omega',m'(\Omega,m)}|^4\Bigg\}+\frac{\hbar^2}{2J}c^*_{\Omega,m}[I(I+1)-\Omega^2] \\
& - \frac{\hbar^2}{2J}\Bigg\{\sum_{m'} c^*_{\Omega+1,m'}[(I-\Omega)(I+\Omega+1)]^{1/2}[u_{\Omega,m(\Omega+1,m')}u_{\Omega+1,m'(\Omega,m)}+v^*_{\Omega,m(\Omega+1,m')}v_{\Omega+1,m'(\Omega,m)}] \\
& \times\langle\Omega+1,m'|j_+|\Omega,m\rangle T_{\Omega+1,m',\Omega,m}+\sum_{m'} c^*_{\Omega-1,m'}[(I+\Omega)(I-\Omega+1)]^{1/2} \\
& \times[u_{\Omega,m(\Omega-1,m')}u_{\Omega-1,m'(\Omega,m)}+v^*_{\Omega,m(\Omega-1,m')}v_{\Omega-1,m'(\Omega,m)}]\langle\Omega-1,m'|j_-|\Omega,m\rangle T_{\Omega-1,m',\Omega,m}\Bigg\} \\
& - i\hbar c^*_{\Omega,m}\Bigg[\sum_{(\Omega',m')\neq(\Omega,m)}\frac{1}{2}(v^*_{\Omega',m'(\Omega,m)}\dot{v}_{\Omega',m'(\Omega,m)}-\dot{v}^*_{\Omega'm'(\Omega,m)}v_{\Omega',m'(\Omega,m)})\Bigg]+\sum_{m'\neq m}h_{\Omega,m',m}c^*_{\Omega,m'},
\end{aligned}
\tag{13}
$$

To obtain the preceding equations, one takes into account the condition of conservation $\sum_{\Omega,m}|c_{\Omega,m}|^2=1$, so that $\sum_{\Omega,m}c_{\Omega,m}\dot{c}^*_{\Omega,m}=-\sum_{\Omega,m}c^*_{\Omega,m}\dot{c}_{\Omega,m}$. It is possible to solve only the equations for positive values of Ω. The interactions between the states $\Omega=1/2$ and their time reversed ones are obsoletes because the flows of probabilities in both directions are the same. Therefore the probabilities of finding a system in a configuration $\Omega=1/2$ or $\bar{\Omega}=-1/2$ remain unchanged.

It should be noticed that for a given configuration, the well known time-dependent pairing equations emerge if the functional (10) is derived with respect the $v_{\Omega,m}$ or $v^*_{\Omega,m}$:

$$
\begin{aligned}
-i\hbar\dot{v}^*_{\Omega',m'(\Omega,m)} = {} & 2v^*_{\Omega',m'(\Omega,m)}(\epsilon_{\Omega',m'}-\lambda)-G\sum_{(\Omega'',m'')\neq(\Omega,m)}\Bigg\{u_{\Omega'',m''(\Omega,m)}v^*_{\Omega'',m''(\Omega,m)}\Bigg(u_{\Omega',m'(\Omega,m)}-\frac{v_{\Omega',m'(\Omega,m)}v^*_{\Omega',m'(\Omega,m)}}{2u_{\Omega',m'(\Omega,m)}}\Bigg) \\
& - u_{\Omega'',m''(\Omega,m)}v_{\Omega'',m''(\Omega,m)}\frac{v^*_{\Omega',m'(\Omega,m)}v^*_{\Omega',m'(\Omega,m)}}{2u_{\Omega',m'(\Omega,m)}}\Bigg\}-2Gv_{\Omega',m'(\Omega,m)}v^*_{\Omega',m'(\Omega,m)}v^*_{\Omega',m'(\Omega,m)}.
\end{aligned}
\tag{14}
$$

Equations (14) can be recast in terms of the single-particle densities $\rho_{\Omega,m(\Omega',m')}=|v_{\Omega,m(\Omega',m')}|^2$ and pairing moment components $\kappa_{\Omega,m(\Omega',m')}=u_{\Omega,m(\Omega',m')}v_{\Omega,m(\Omega',m')}$ [28,29], yielding a system similar to the time-dependent Hartree-Fock-Bogoliubov equations [30–34]. These time-dependent pairing equations can be generalized to study the partition of the excitation energy between two complementary fragments by adding a condition of conservation of the number of particles [35,36].

From the time-dependent pairing equations (14), the time derivatives of $v_{\Omega,m}$ are provided and the relation

$$
\begin{aligned}
\frac{i\hbar}{2}(v^*_{\Omega',m'(\Omega,m)}\dot{v}_{\Omega',m'(\Omega,m)}-\dot{v}^*_{\Omega',m'(\Omega,m)}v_{\Omega',m'(\Omega,m)}) = {} & 2|v_{\Omega',m'(\Omega,m)}|^2(\epsilon_{\Omega',m'}-\lambda)-2G|v_{\Omega',m'(\Omega,m)}|^4 \\
& + \mathrm{Re}\Bigg\{\Delta^*_{\Omega,m}\Bigg(\frac{|v_{\Omega',m'(\Omega,m)}|^4}{u_{\Omega',m'(\Omega,m)}v^*_{\Omega',m'(\Omega,m)}}-u_{\Omega',m'(\Omega,m)}v_{\Omega',m'(\Omega,m)}\Bigg)\Bigg\}
\end{aligned}
\tag{15}
$$

is obtained. Therefore, the time derivative $\dot{v}_{\Omega',m'(\Omega,m)}$ can be eliminated from Eqs. (13). Here, $\Delta_{\Omega,m}=G\sum_{(\Omega',m')\neq(\Omega,m)}u_{\Omega',m'(\Omega,m)}v_{\Omega',m'(\Omega,m)}$ is the pairing gap parameter of the configuration (Ω,m).

Equations (13), completed with the equality (15), illustrate two inherent mixing mechanisms between different seniority-1 configurations that occur in dynamical systems. The first one is the Coriolis interaction. In an axially symmetric system, this interaction acts between states that differ by one unit in the values of Ω. These configuration mixings are produced by the nonvanishing matrix elements $\langle\Omega',m'|j_\pm|\Omega,m\rangle$. The second mixing mechanism is the Landau-Zener effect. The interaction that causes this promotion mechanism manifests itself only between single-particle states that have the same good quantum numbers in the avoiding crossing regions. This effect is taken into consideration in the time-dependent equations by means of the interactions $h_{\Omega,m',m}$. If the pairing interaction vanishes, the system (13) can be particularized to the time-dependent equations of Ref. [14] deduced only for single-particle systems.

The energies of the many-body Hamiltonian H are

$$E_{\Omega,m} = \langle\varphi_{IM\Omega m}|H|\varphi_{IM\Omega m}\rangle = 2\sum_{(\Omega',m')\neq(\Omega,m)}|v_{\Omega',m'(\Omega,m)}|^2(\epsilon_{\Omega',m'}-\lambda)+(\epsilon_{\Omega,m}-\lambda)-\frac{|\Delta_{\Omega,m}|^2}{G}-G\sum_{(\Omega',m')\neq(\Omega,m)}|v_{\Omega',m'(\Omega,m)}|^4, \tag{16}$$

and the centrifugal ones are

$$E^{\mathrm{R}}_{I,\Omega} = \langle\varphi_{IM\Omega m}|\frac{\hbar^2}{2J}\left(I^2-j_z^2\right)|\varphi_{IM\Omega m}\rangle = \frac{\hbar^2}{2J}[I(I+1)-\Omega^2], \tag{17}$$

where $|\varphi_{IM\Omega m}\rangle$ are wave functions of the superposition (2). Both energies intervene in Eqs. (13).

In order to determine the probabilities of the possible seniority-1 configurations stemming from the α decay process, the system (13) should be solved, starting from the ground state and reaching the scission. The time-dependent variables of my equations are the amplitudes of the seniority-1 configurations and those of the BCS functions. In the literature, the equations of motion are usually given in terms of probabilities. Therefore, for completeness Eqs. (13) and (14) are also recast in terms of probabilities instead of amplitudes in the Appendix. At scission, the the probabilities $P_{\Omega,m} = |c_{\Omega,m}|^2$ should give information compatible with those deduced from the overlap probabilities for different excited states (or seniority-1 configurations) of the daughter [37,38].

III. RESULTS AND DISUSSION

In order to solve the equations of motion, the rearrangement of the single-particle levels $\epsilon_{\Omega,m}$ should be provided beginning from the ground state and reaching the scission point. The time evolution of the mean field potential is required for this purpose. In most treatments of nuclear fission, this potential is constrained by a nuclear shape parametrization characterized by some degrees of freedom [39]. The generalized coordinates associated with these degrees of freedom are forced to vary along a path in the multidimensional configuration space, leading finally to a split of the nuclear system [40] into two bodies. Such a fission trajectory can be obtained according to the least action principle, by calculating the minimal values of the action integral between the ground state of the parent nucleus and a scission configuration compatible with the α-decay process. The action integral requires the evaluation of the deformation energy and of the inertia. In this work, the deformation energy was computed in the framework of the macroscopic-microscopic approach [41,42], while the nuclear inertia was calculated within the cranking model [43,44]. In the cranking model, the nucleons move freely in a mean field potential subject to an external motion [45,46]. In the macroscopic-microscopic formalism it is postulated that a macroscopic theory describes quantitatively the smooth trends of the total nuclear energy with respect to the deformations while the microscopic effects are responsible for the local fluctuations. The macroscopic deformation energy is calculated within the finite-range liquid-drop model [47,48] extended for binary systems. The microscopic shell and pairing corrections were obtained by mean of the Strutinsky procedure [49] based on a mean field solved by the Woods-Saxon two-center shell model [23], using the so-called universal parametrization for the potential [50]. The orthogonal eigenvalue basis is obtained by diagonalizing the Woods-Saxon mean field in the semisymmetric two-center harmonic potential basis [51–53]. The matrix elements for the derivative of the potential required to calculate the inertia are also obtained with the same wave functions. For a fixed major quantum number, the two-center shell model provides the lower energy single-particle wave functions for any internuclear distance between two separated fragments. Molecular states that characterize scission configurations can be precisely described. Due to this advantage, different versions of the two-center shell model are used in the literature to treat processes such as nuclear disintegrations or collisions [54–56]. My nuclear shape parametrization should provide a smooth transition between one parent nucleus and a two-body nuclear configuration. This behavior is obtained with an axially symmetric nuclear shape parametrization given by two spheroids joined by an intermediate surface simulating the neck [23]. This intermediate surface is obtained by rotating an arc of a circle tangent to both spheroids around the axis of symmetry. Five degrees of freedom characterize this nuclear shape parametrization: the elongation defined by the internuclear distance R between the centers of the spheroids, the necking parameter that can be measured by the curvature $C = s/R_3$ of the intermediate surface (R_3 and s being the radius of the arc of circle and the sign of the curvature, respectively), the mass asymmetry that can be considered as the ratio of the major semiaxes of the two spheroids, and the deformations of both fragments characterized by their eccentricities. The minimization of the action integral is performed numerically as described in Ref. [57]. First of all, the ground state of the parent is determined by calculating the lowest deformation energy, while the scission point is considered as the touching configuration of a dinuclear system consisting of the spherical nuclei ^{207}Pb and ^{4}He. The elongations for the initial and the final configurations are therefore established. One defines a trajectory between these points that is approximated by a spline function. This spline function depends on several values of the generalized coordinates in different mesh points fixed along the elongation parameter. So, the action integral in the WKB approximation [40] becomes now a function that depends on the values of the generalized coordinates considered as variables. A numerical minimization can be now performed to obtain the least action trajectory. Such kinds of calculations were already performed for fission [58–60], cluster emission [61,62], and α decay [63,64]. The potential barrier V for α decay along the least action trajectory is plotted

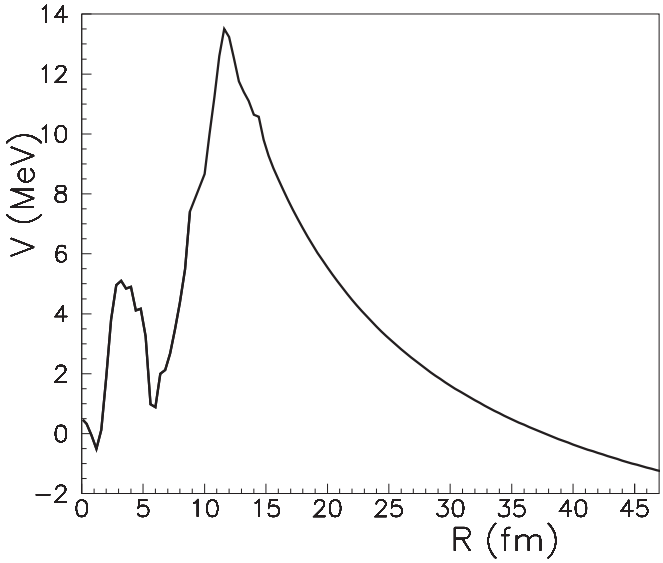

FIG. 1. The deformation energy V as function of the internuclear distance R for α decay. The height of the barrier is renormalized by taking into account a zero-point vibration energy of 0.5 MeV.

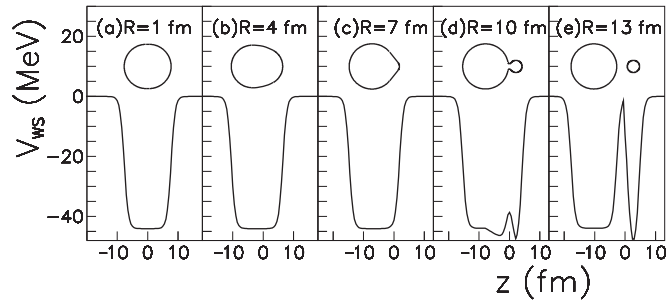

FIG. 2. The Woods-Saxon potential V_{WS} for the α-particle emission as a function of the axial cylindrical coordinate z is displayed for several internuclear distances R. The internuclear distances are marked on the plots. The corresponding nuclear shapes are also represented at the top of each panel.

in Fig. 1. A pocket in the potential is formed around the scission configuration. The origin of this pocket was explained in Ref. [64]. The strong stabilizing shell effects of the nearly spherical daughter produce a molecular minimum where the α particle is preformed on the surface. A similar potential pocked was introduced phenomenologically in Ref. [65] in order to improve the agreement between theory and experimental α decay widths. In the presence of the potential pocket displayed in Fig. 1, the α-decay potential barrier resembles formally the double-humped barrier encountered in fission. In fission, the double-humped barrier is responsible for the β vibrational transitions created by collective resonances in the second minimum. Speculating on this similarity, it is also possible to consider that the pure α-cluster states obtained experimentally from non-natural transitions in Ref. [66] could be due to collective vibrational resonances in the α-decay second well of the potential. The Woods-Saxon potentials and the corresponding nuclear shapes during the decay process are displayed in Fig. 2. As mentioned, the same "universal" Woods-Saxon parametrization was used for the parent nucleus, the daughter one, and the α particle.

The single-particle diagrams as a function of the elongation R are displayed in Fig. 3 for neutrons and in Fig. 4 for protons. The ground state is located around at $R_{gs} \approx 0.8$ fm. The single-particle states of the ^{211}Po nucleus, considered to be spherical, are assigned on the left with their spectroscopic notations. At an elongation R_s of about 10 fm, a dinuclear system consisting of the ^{207}Pb spherical daughter nucleus and the α particle is obtained. Accordingly, the single-particle levels are rearranged as function of the internuclear distance R, resulting in a superposition of the single-particle level belonging to the α particle (marked with $1s_{1/2}$ on the right of the Figs. 3 and 4) with the single-particle level scheme of the daughter. In the case of protons, the electrostatic repulsion between the formed nuclei leads to a decrease of the single-particle energies when the nuclei get away one from another. The slope for the variation of the single-particle energy of the α particle is more evident than those belonging to the daughter nucleus. As displayed in Fig. 3 concerning the neutron diagram, the single-particle level emerging from the

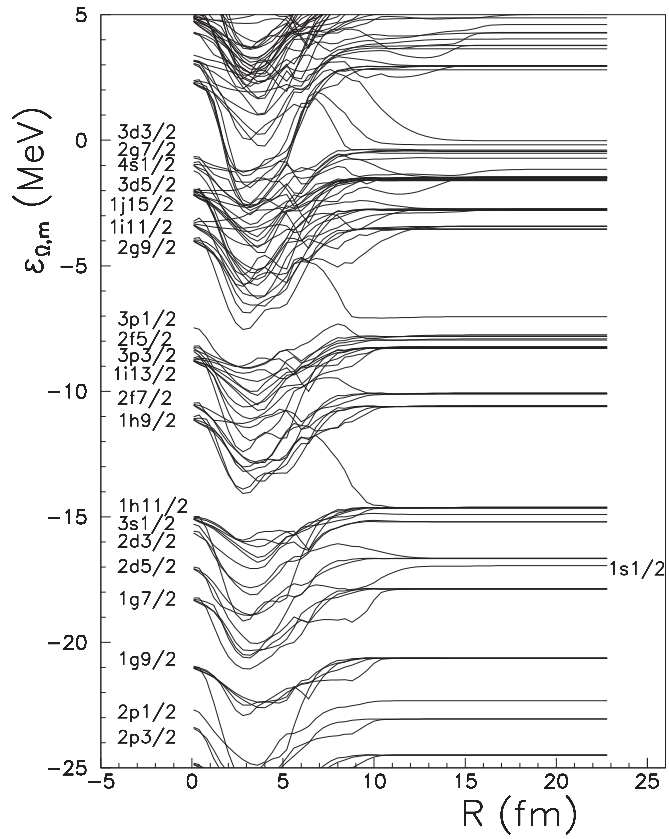

FIG. 3. Neutron single-particle energies as a function of the distance between the centers of the fragments R. The single-particle levels of the spherical parent nucleus are labeled with their spectroscopic notations on the left side. After the scission produced at $R \approx 10$ fm, the single-particle levels of the daughter nucleus are superimposed on the single-particle level belonging to the α particle, labeled on the right side with the spectroscopic notation $1s_{1/2}$.

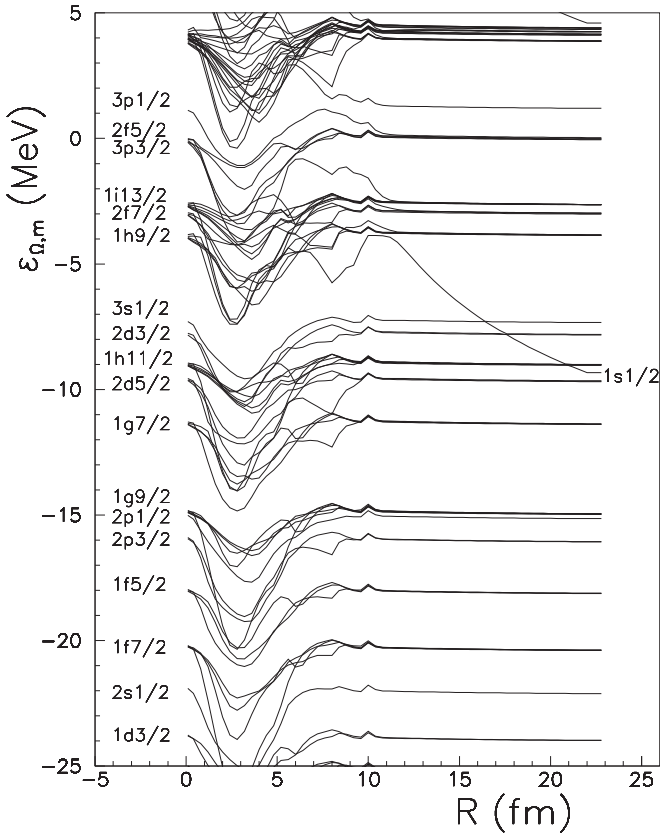

FIG. 4. Proton single-particle energies. The single-particle levels of the parent are labeled on the left with their spectroscopic notations. The single-particle level pertaining to the α particle is marked on the right.

parent state $2d_{5/2}$ with the spin projection $\Omega = 1/2$ approaches asymptotically to the orbital $1s_{1/2}$, centered in the potential well of the α particle. That is, during the rearrangement of the level diagram, one single-particle level is extracted from the parent nucleus to constitute the α particle. Therefore, the daughter final state $\Omega = 1/2$ of the orbital $2d_{5/2}$ should be filled by superior levels belonging to the same $\Omega = 1/2$ subspace. That is, the superior $\Omega = 1/2$ level should replace in the daughter fragment the single-particle level extracted by the α particle. Indeed, the single-particle level emerging from the parent $2d_{3/2}$ replaces the $2d_{5/2}$ orbital of the daughter. Successive replacements are produced up to a complete filling of all orbitals of the daughter nucleus. The evolutions as function of R of some selected neutron single-particle levels around the Fermi energy, and hence participating to the mixing configuration process, are presented in Fig. 5. All these levels pertain to the subspace $\Omega = 1/2$. Their variation illustrates how the successive replacements are produced by filling free orbitals of the daughter at scission. In panel (a) of Fig. 5, it can be observed that the neutron located in the last occupied orbital of the parent nucleus denoted $2g_{9/2}$ will arrive adiabatically, after the emission of the α particle, at the state $3p_{1/2}$ of the daughter. At the same time, the superior single-particle level emerging from $1i_{11/2}$ reaches the state $2g_{9/2}$. In the panels (d) and (g), in a similar manner the levels emerging from $3p_{1/2}$ and $2f_{5/2}$ will be finally located in the states $2f_{5/2}$ and $3p_{3/2}$ of the daughter nucleus, respectively. During the rearrangements of these single-particle levels, some avoided level crossing regions should be produced. Such regions could be identified by evaluating the differences between the energies of two adjacent single-particle levels $\Delta\epsilon = \epsilon_{\omega,m} - \epsilon_{\Omega,m-1}$. In general, the avoided level crossing regions are characterized by some minimal values of these differences. Such differences are plotted in panels (b), (e), and (h), corresponding to the levels selected on the left side of the figure. The possible avoided level crossing regions are marked with arrows. In order to confirm the fact that these minima identify avoided level crossing regions without ambiguities, I calculated also the total intrinsic spins $j_{\Omega,m}$ of the microscopic states (Ω,m) [from the equation $j_{\Omega,m}(j_{\Omega,m}+1) = \langle\Omega,m \mid j^2|\Omega,m\rangle$]. The variation of the total intrinsic spin is plotted in the panels (c), (f), and (i). In a true avoided level crossing region, the levels should exchange their characteristics. For example, in atomic physics, a pure polar electron state can become homopolar after the passage of an avoided crossing, as remarked by Zener [21]. As indicated by the arrows, the avoided level crossing regions are located at the same internuclear distances as the intersections of the values of the total intrinsic spins $j_{\Omega,m}$ in panels (f) and (i). No intersections can be noticed in panel (c), therefore one concludes that the minima marked with arrows in panel (b) are not consistent with the existence of avoided level crossing regions. Moreover, the initial and final values of the total intrinsic spin are consistent with the spectroscopic notations used to label the initial and final states of the single-particle levels. The formalism of for the ladder operators in the framework of the Woods-Saxon two-center shell model is given in Ref. [44].

The magnitude of the interaction in the avoided level crossing regions is evaluated as described in Ref. [24]. By using some interpolation procedures, the behavior of the diabatic single-particle levels can be determined. The energy differences between the adiabatic and the diabatic states offer an estimation for the Landau-Zener interaction.

The unpaired nucleon, initially emerging from the state $2g_{9/2}$ with $\Omega = 1/2$ will mainly traverse two avoided level crossing regions: the region located at $R \approx 8.77$ fm between the adiabatic levels emerging from $2g_{9/2}$ and $3p_{1/2}$, and another one located at $R \approx 9.97$ fm between the adiabatic levels emerging from $3p_{1/2}$ and $2f_{5/2}$. If the nucleon follows diabatic states, it will skip from one single-particle level to another in each avoided level crossing region. That is, for large internuclear velocities $\dot{R}$, the nucleon initially located in the parent state $2g_{9/2}$ should arrive with a very large probability at the final daughter state $3p_{3/2}$. For small internuclear velocities, the nucleon should follow adiabatically the same single-particle level, to arrive at the final state $3p_{1/2}$ of the daughter nucleus. In this situation, one retrieves the ground state configuration of the daughter nucleus. For intermediate velocities, all the three final states $3p_{1/2}$, $2f_{5/2}$, and $3p_{3/2}$ can be occupied with different probabilities by the unpaired nucleon. These probabilities can be obtained by solving the system of equations of motion (13).

I selected several single-particle levels around the Fermi energy in order to investigate the mixing configuration

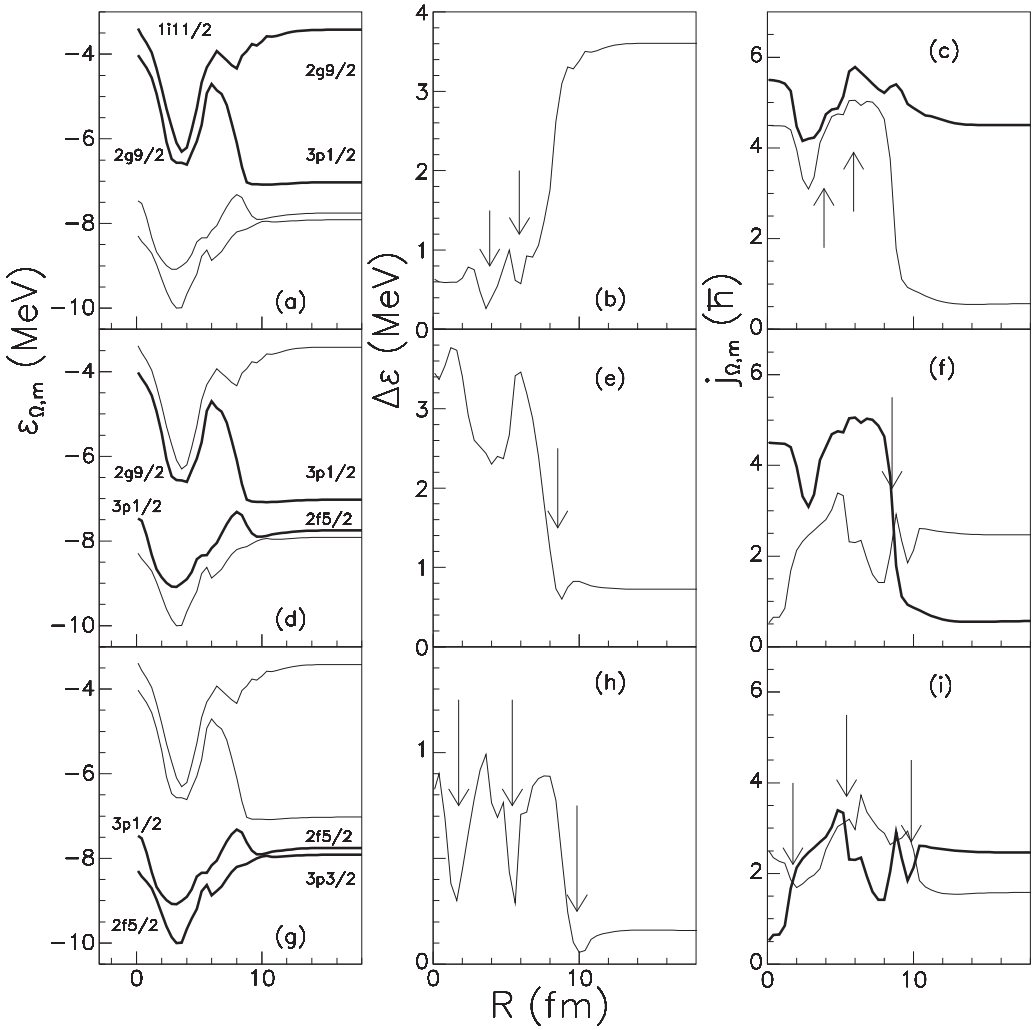

FIG. 5. The variations of several single-particle levels $\epsilon_{\Omega,m}$ located around the Fermi energy as a function of the internuclear distance R are displayed in panels (a), (d), and (g). The spin projection of these levels is $\Omega = 1/2$. In each panel two adjacent single-particle levels are selected and are plotted with a thick line. They are labeled with their spectroscopic notations corresponding to the parent on the left and to the daughter on the right. The differences in energies $\Delta\epsilon = \epsilon_{\Omega,m} - \epsilon_{\Omega,m-1}$ are plotted on the panels (b), (e), and (h) for the two adjacent single-particle levels selected in the panels (a), (d), and (g), respectively. Minimum values of these differences should locate the avoided crossing regions. These minima are marked with arrows. The total intrinsic spins $j_{\Omega,m}$ of the single-particle levels selected in the panels (a), (d), and (g) are displayed in the panels (c), (f), and (i), respectively. The total intrinsic spin corresponding to the superior single-particle level is plotted with a thick line. The arrows indicate the locations of the avoided level crossing regions. The values of $j_{\Omega,m}$ intersect in the same regions in panels (f) and (i).

mechanism; they are tabulated in Table I. Excepting the internuclear velocity, all the ingredients required to solve Eqs. (13) are available, being supplied by the variations of the single-particle energies or calculated in terms of the wave functions that result form the Woods-Saxon two-center shell model. Only the internuclear velocity $\partial R/\partial t$ is missing. Different values of the internuclear velocities ranging from 10^4 to 10^6 fm/fs were tested to reproduce the fine structure and to estimate the disintegration time.

In the external region, the two nuclei move away from each other. The moment of inertia increases proportionally with the square of the internuclear distance. Therefore the Coriolis interaction becomes very small. In the external region as well, the single-particle energies remain unchanged and one no longer has avoided level crossing regions. From these reasons, configuration changes are no longer produced.

The fine structure of ^{211}Po α decay is characterized by 98.9% transitions to the $3p_{1/2}$ ground state of the daughter, 0.55% to the $2f_{5/2}$ first single-particle excited state, and 0.54% to the $3p_{3/2}$ second single-particle excited state [67,68]. The ground state configuration of the parent nucleus ^{211}Po is $[\pi(h_{9/2})^2\nu(g_{9/2})^1]_{9/2^+}$ [69]. So, the unpaired neutron emerges from the level $2g_{9/2}$ and the total spin of the system is $I = 9/2\,\hbar$.

The system (13) is solved by starting from the ^{211}Po ground state, located at $R_{gs} \approx 0.8$ fm, and arriving at the scission point $R_s \approx 10$ fm. For the seniority-1 configurations (Ω,m) listed in Table I, the initial occupation $v_{\Omega',m'(\Omega,m)}$ and vacancy $u_{\Omega',m'(\Omega,m)}$ amplitudes correspond to the respective solutions of the BCS stationary equations. The initial amplitude is $c_{\Omega=1/2,3p_{1/2}} = 1$ for the seniority-1 configuration in which the $\Omega = 1/2$ blocked level emerges from the $2g_{9/2}$ parent orbital

and reaches the $3p_{1/2}$ daughter orbital. This corresponds to a transition from the ground state of the parent nucleus to the ground state of the daughter one. The amplitudes $c_{\Omega,m}$ for the remaining configurations are initially constrained to be zero. The system (13) is solved for different values of the internuclear velocities. I obtained the amplitudes $c_{\Omega,m}$ for the realization of different (Ω,m) seniority-1 configurations as functions of the elongation. The absolute square $P_{\Omega,m} = |c_{\Omega,m}|^2$ at the scission R_s has a meaning similar to the overlap probability for final excitations (Ω,m). Equations (13) conserve the total probability, as can be verified from Table I, with the sum over the considered single-particle levels satisfying the condition $\sum P_{\Omega,m} = 1$.

The partial half-life for one transition state pertaining to a seniority-1 configuration (Ω,m) is inversely proportional to its barrier penetrability $P^{\rm b}_{\Omega,m}$ and to its probability of achieving the configuration $P_{\Omega,m} = |c_{\Omega,m}|^2$ at scission [70]:

$$T_{\Omega,m} \propto \left(P^{\rm b}_{\Omega,m} P_{\Omega,m}\right)^{-1}. \tag{18}$$

The penetrability of the barrier is determined in the WKB approximation as

$$P^{\rm b}_{\Omega,m} = \exp\left\{-\frac{2}{\hbar}\int_{R_s}^{R_e}\sqrt{2B(R)\left[V(R) + \left(E_{\Omega,m}(R) - E_{1/2,3p_{1/2}}\right) + E^{\rm R}_{I,\Omega}\right]}dR\right\}. \tag{19}$$

As mentioned, the value of the total orbital momentum is $I = 9/2\,\hbar$, corresponding to the parent ground state. It determines the centrifugal term $E^{\rm R}_{I,\Omega}$ given with the expression (17). V is the deformation energy in the macroscopic-microscopic formalism, displayed in Fig. 1. $E_{1/2,3p_{1/2}}$ is the lowest transition state of the decaying system, pertaining to the $\Omega = 1/2$ Fermi level emerging from the ground state of the parent $2g_{9/2}$ and reaching the ground state of the daughter $3p_{1/2}$. The other transition states have barriers increased by their specialization energies [71], given by the differences $E_{\Omega,m}(R) - E_{1/2,3p_{1/2}}$. Because the energies calculated with the expression (16) contain BCS parameters that are solutions of the system (14), the effect of the dissipated energy is included in these differences [28]. The dissipation means a transfer of energy or angular momentum from collective degrees of freedom into internal ones [72]. The integral is evaluated between the scission point R_s and the exit point of the barrier R_e, which depends on the transition state. B is the effective mass along the superasymmetric fission trajectory, evaluated in the framework of the cranking model.

TABLE I. Selected transition levels around the Fermi energy. The initial and final orbitals and the projections of the intrinsic spin Ω are presented in the first three columns, respectively. The single-particle level $\Omega = 3/2$ emerging from $1i_{11/2}$ reaches the $1p_{3/2}$ state of the α particle. The last column display the probabilities $P_{\Omega,m} = |c_{\Omega,m}|^2$ of the configurations (Ω,m) for an internuclear velocity $v = 2 \times 10^4$ fm/fs at an elongation $R = 10.5$ fm.

Initial state	Final state	Ω	$P_{\Omega,m}$
$1i_{11/2}$	$2g_{9/2}$	1/2	0.102
$2g_{9/2}$	$3p_{1/2}$	1/2	9.553×10^{-2}
$3p_{1/2}$	$2f_{5/2}$	1/2	7.865×10^{-2}
$2f_{5/2}$	$3p_{3/2}$	1/2	8.323×10^{-2}
$1i_{13/2}$	$2f_{7/2}$	1/2	1.898×10^{-5}
$1i_{11/2}$	$1p_{3/2}$-α	3/2	0.207
$2g_{9/2}$	$2g_{9/2}$	3/2	0.1621
$2f_{5/2}$	$2f_{5/2}$	3/2	1.965×10^{-3}
$3p_{3/2}$	$3p_{3/2}$	3/2	1.952×10^{-2}
$1i_{13/2}$	$1i_{13/2}$	3/2	2.067×10^{-3}
$1i_{11/2}$	$1i_{11/2}$	5/2	0.1468
$2f_{5/2}$	$2f_{5/2}$	5/2	5.353×10^{-3}
$1i_{11/2}$	$1i_{11/2}$	7/2	9.661×10^{-2}
$2g_{9/2}$	$2g_{9/2}$	7/2	4.570×10^{-2}
$1i_{13/2}$	$1i_{13/2}$	7/2	1.162×10^{-8}
$1i_{11/2}$	$1i_{11/2}$	9/2	4.331×10^{-2}
$2g_{9/2}$	$2g_{9/2}$	9/2	4.841×10^{-3}
$1i_{13/2}$	$1i_{13/2}$	9/2	3.396×10^{-11}
$1i_{11/2}$	$1i_{11/2}$	11/2	3.977×10^{-8}
$1i_{13/2}$	$1i_{13/2}$	11/2	4.701×10^{-11}

The ^{207}Pb daughter nucleus is considered spherical. So, the single-particle states are degenerate in the intrinsic spin projection Ω. The partial half-life for only one excitation m of the daughter nucleus considered spherical is given by the contributions of all transition states of different spin projections Ω that reach the same degenerate seniority-1 configuration. That is, the partial half-life for one final excitation m in the spherical daughter nucleus is given by the formula

$$\frac{1}{T_m} = \sum_{\Omega}\frac{1}{T_{\Omega,m}}. \tag{20}$$

For example, the partial half-life for the final daughter state $2g_{9/2}$ can be calculated as

$$\frac{1}{T_{2g_{9/2}}} = \frac{1}{T_{1/2,2g_{9/2}}} + \frac{1}{T_{3/2,2g_{9/2}}} + \frac{1}{T_{5/2,2g_{9/2}}} + \frac{1}{T_{7/2,2g_{9/2}}} + \frac{1}{T_{9/2,2g_{9/2}}}, \tag{21}$$

within the seniority-1 configurations selected in Table I. The yield for the final configuration $2g_{9/2}$ is $Y_{2g_{9/2}} = T/T_{2g_{9/2}} \times 100$ in percent, where T is the total half-life. Now, the yields of the fine structure can be obtained in the same way for other excited states of the daughter nucleus. The partial half-life for the ground state of the daughter is given only by the transition to the $3p_{1/2}$ state of the single-particle level with spin projection $\Omega = 1/2$ emerging from the parent orbital $2g_{9/2}$.

Several values for the internuclear velocity $v = dR/dt$ were tested in order to reproduce the fine structure parameters. The value $v = 2 \times 10^4$ fm/fs gives the best agreement between the theory and the experiment. The probabilities of the

TABLE II. Yields Y for the fine structure, in percent, for different values of the internuclear velocity v. The spectroscopic notations label the final state of the daughter (or of the emitted particle).

v (fm/fs)	$Y_{1i_{11/2}}$ (%)	$Y_{2g_{9/2}}$ (%)	$Y_{3p_{1/2}}$ (%)	$Y_{2f_{5/2}}$ (%)	$Y_{3p_{3/2}}$ (%)	$Y_{1i_{13/2}}$ (%)	$Y_{2f_{7/2}}$ (%)	$Y_{1p_{3/2}\alpha}$ (%)
0.9×10^4	1.28×10^{-21}	1.21×10^{-14}	85.38	2.97	11.63	2.98×10^{-4}	4.88×10^{-19}	1.5×10^{-22}
2×10^4	1.41×10^{-23}	2.34×10^{-15}	99.10	0.26	0.62	8.25×10^{-4}	7.62×10^{-18}	2.30×10^{-24}
3×10^4	9.85×10^{-22}	4.08×10^{-13}	99.66	1.59×10^{-2}	0.32	3.69×10^{-4}	3.47×10^{-18}	1.84×10^{-22}
4×10^4	3.69×10^{-24}	4.69×10^{-16}	97.89	1.20	0.89	2.34×10^{-3}	2.25×10^{-19}	6.30×10^{-25}

seniority-1 configurations are listed in Table I. The yields obtained theoretically are presented in Table II, together with the results obtained for other velocities. I obtained theoretically 99.1% transitions to the ground state, 0.26% transitions to the first excited state, and 0.62% transitions to the second excited state. It is interesting to note that the theory also predicts the emission of ^{5}He with a very small probability. The agreement between the experimental data and the theory is very good, keeping in mind that the parameters of the model are not adjusted at all. The Q value is obtained within the macroscopic-microscopic model and the single-particle energies are given by the Woods-Saxon two-center shell model alone. The time to penetrate the barrier is about 1.7×10^{-18} s, leading to a very large disintegration time.

In fission, the scission time is still a subject of debate. For example, as discussed in Ref. [44], some Hartree-Fock calculations predict mean velocities around the scission point of the order of 1×10^6 fm/fs [33,73,74], while models that take into consideration state dependent pairing interactions gives values of the order of $6 \times 10^4 - 2 \times 10^5$ fm/fs [75]. A good agreement between the experimental value of the spontaneous fission half-life and the theory was obtained for a mean velocity 1×10^5 in Ref. [44]. A similar situation can be encountered in the case of the α-decay process. The time scale predictions for the α tunneling are model dependent. For example, in Ref. [76] it was calculated that the time spent by the nuclear system before entering the barrier and the half-life of the α decay are of the same order of magnitude. That is, very slow processes can be considered. On the other hand, the tunneling velocity deduced in Ref. [77] by solving the time-dependent Schrodinger equation for metastable initial states is of the order of 10^7 fm/fs.

IV. CONCLUSIONS

A new system of equations of motion is deduced from the variational principle. These equations can be easily particularized to the time-dependent pairing equations if the configuration mixing mechanism is neglected. As noticed in Ref. [23], these equations can be also particularized to the Landau-Zener differential equations for pure single-particle systems, when the pairing interaction and the Coriolis coupling are neglected. When only the pairing interaction is neglected, the system of equations presented in Ref. [14] is retrieved. Therefore, this new system of equations represents a generalization of the time-dependent pairing equations able to mix seniority-1 configurations. The probability of obtaining a given configuration is determined dynamically.

These equations are solved for a simple case, the α decay of ^{211}Po, in order to explain the fine structure phenomenon. A very good agreement between the theory and the experiment was obtained. A mean value of the tunneling velocity of about $v = 2 \times 10^4$ fm/fs was predicted. The calculations show that the emission of ^{5}He is also possible with a very small probability.

Usually, the favored transitions in the α decay of odd nuclei proceed to daughter states with the same quantum numbers as the parent ones. In the case of the ^{211}Po α decay, the transitions to the ground state are favored due to the Landau-Zener promotion mechanism. Concerning the proton single-particle diagram displayed on Fig. 4, it can be noticed that an avoided level crossing region occurs at $R \approx 8$ fm and $E = -6.5$ MeV between two single-particle levels with the same value $\Omega = 1/2$. These levels emerge from the parent orbitals $1h_{9/2}$ and $3s_{1/2}$. The Landau-Zener promotion mechanism can also be responsible for the enhanced branch $9/2^- \rightarrow 1/2^+$ in the α decay of ^{211}Bi.

In my treatment, the α decay is considered as a superasymmetric fission process. That is, a fission path is calculated in a multidimensional configuration space, paying attention to the structure aspects of the potential energy and to the variations of the inertia up to the scission configuration. The variation of the nuclear structure is analyzed during the whole disintegration process and dynamical single-particle effects are evidenced. There are several models in the literature where it is claimed that the α decay is treated like a fission process. In all these approaches, the ground state of the parent is defined only from an energy point of view, by reproducing only the experimental Q value of the reaction, readjusted by an zero-point vibration energy. No deformations are associated with this parent ground state. The variation of the deformation energy is usually fitted in a rudimentary way by using some interpolating functions in order to reproduce the height of the Coulomb barrier at scission. In some models, finite range nuclear terms are also used to improve the energy around the scission configuration, as in, for example, the proximity potential [78] or the Yukawa plus exponential surface term [79]. Sometimes, the liquid drop energy is used to evaluate the variation of the deformation energy in the overlap region by involving very simple nuclear shape parametrizations, but phenomenological shell corrections are introduced to reproduce the Q value [80]. These kinds of approaches consider that the effective mass in the overlap region is equal to the reduced mass where the two fragments are separated. The major part of the penetrability calculated for α decay is obtained from the external region, the overlap region being of little importance.

For two separated bodies, only the Coulomb field and the reduced mass intervene. Because the height of the external barrier is fixed by the experimental Q value, in principle, the systematic behavior of calculated half-lives should be in agreement with the experimental ones. Indeed, many practical formulas for α half-life systematics are based on very simple formulas involving the Q value [81–83]. It is true that also in fission it is possible to introduce some double humped parametrized barriers in order to estimate the heights of the barriers. But, due to the fact that the scission point is located in the external region of the barrier, it is not possible to relate this barrier to the Q-value to estimate the half-life of the process. So, in fission treatments the variations of the energy and of the mass in the overlap regions are of crucial importance and determine the spontaneous half-life. In a true fission-like model, the overlap region should be investigated carefully and its properties should be calculated. In my dynamical treatment in the framework of the superasymmetric fission model, one takes into account the properties of the parent ground state and the variation of the deformation energy (including corrections due to the structure) and of the inertia along the fission path. So, my treatment for α decay is really a fission-like one.

ACKNOWLEDGMENTS

This work was supported by grants of Romanian Ministery of Research and Innovation, CNCS-UEFISCDI, Projects No. PN-III-P4-ID-PCE-2016-0092 and No. PN-III-P4-ID-PCE-2016-0014, within PNCDI III.

APPENDIX

Equations (14) can be rewritten in terms of single-particle densities $\rho_{\Omega,m(\Omega',m')} = |v_{\Omega,m(\Omega',m')}|^2$ and pairing moment components $\kappa_{\Omega,m(\Omega',m')} = u_{\Omega,m(\Omega',m')}v_{\Omega,m(\Omega',m')}$ as

$$\begin{aligned} i\hbar\dot{\rho}_{\Omega,m(\Omega',m')} &= \kappa_{\Omega,m(\Omega',m')}\Delta^*_{\Omega,m} - \kappa^*_{\Omega,m(\Omega',m')}\Delta_{\Omega,m}, \\ i\hbar\dot{\kappa}_{\Omega,m(\Omega',m')} &= (2\rho_{\Omega,m(\Omega',m')} - 1)\Delta_{\Omega,m} + 2\kappa_{\Omega,m(\Omega',m')}(\epsilon_{\Omega,m} - \lambda) - 2G\rho_{\Omega,m(\Omega',m')}\kappa_{\Omega.m(\Omega',m')}. \end{aligned} \tag{A1}$$

Similarly, Eqs. (13) can be rewritten in terms of the probabilities $P_{\Omega,m} = |c_{\Omega,m}|^2$ of the configurations (Ω,m) and the mixing moment components between configurations $S_{(\Omega,m)(\Omega',m')} = c_{\Omega,m}c^*_{\Omega',m'}$. These equations are

$$\begin{aligned} i\hbar\dot{P}_{\Omega,m} = &-\frac{\hbar^2}{2J}\Bigg\{\sum_{m'}[S_{(\Omega,m)(\Omega+1,m')} - S_{(\Omega+1,m')(\Omega,m)}][(I-\Omega)(I+\Omega+1)]^{1/2} \\ &\times\left[\sqrt{\frac{|\kappa_{\Omega,m(\Omega+1,m')}|^2}{\rho_{\Omega,m(\Omega+1,m')}}\frac{|\kappa_{\Omega+1,m'(\Omega,m)}|^2}{\rho_{\Omega+1,m'(\Omega,m)}}} + \kappa^*_{\Omega,m(\Omega+1,m')}\kappa_{\Omega+1,m'(\Omega,m)}\sqrt{\frac{\rho_{\Omega,m(\Omega+1,m')}}{|\kappa_{\Omega,m(\Omega+1,m')}|^2}\frac{\rho_{\Omega+1,m'(\Omega,m)}}{|\kappa_{\Omega+1,m'(\Omega,m)}|^2}}\right] \\ &\times\langle\Omega+1,m'|j_+|\Omega,m\rangle T_{\Omega+1,m',\Omega,m} + \sum_{m'}[S_{(\Omega,m)(\Omega-1,m')} - S_{(\Omega-1,m')(\Omega,m)}][(I+\Omega)(I-\Omega+1)]^{1/2} \\ &\times\left[\sqrt{\frac{|\kappa_{\Omega,m(\Omega-1,m')}|^2}{\rho_{\Omega,m(\Omega-1,m')}}\frac{|\kappa_{\Omega-1,m'(\Omega,m)}|^2}{\rho_{\Omega-1,m'(\Omega,m)}}} + \kappa^*_{\Omega,m(\Omega-1,m')}\kappa_{\Omega-1,m'(\Omega,m)}\sqrt{\frac{\rho_{\Omega,m(\Omega-1,m')}}{|\kappa_{\Omega,m(\Omega-1,m')}|^2}\frac{\rho_{\Omega-1,m'(\Omega,m)}}{|\kappa_{\Omega-1,m'(\Omega,m)}|^2}}\right] \\ &\times\langle\Omega-1,m'|j_+|\Omega,m\rangle T_{\Omega-1,m',\Omega,m}\Bigg\} + \sum_{\Omega,m'}^{n} h_{\Omega,m',m}[S_{(\Omega,m)(\Omega,m')} - S_{(\Omega,m')(\Omega,m)}], \end{aligned} \tag{A2}$$

and

$$\begin{aligned} i\hbar\dot{S}_{(\Omega,m)(\Omega_1,m_1)} = S_{(\Omega,m)(\Omega_1,m_1)}\Bigg\{&\frac{\hbar^2}{2J}(\Omega^2-\Omega_1^2) + -\frac{1}{G}\left(|\Delta_{\Omega_1,m_1}|^2 - |\Delta_{\Omega,m}|^2\right) + (\epsilon_{\Omega_1,m_1} - \epsilon_{\Omega,m} - 2\lambda) \\ &+ G\left(\sum_{(\Omega',m')\neq(\Omega_1,m_1)}\rho^2_{\Omega',m'(\Omega_1,m_1)} - \sum_{(\Omega',m')\neq(\Omega,m)}\rho^2_{\Omega',m'(\Omega,m)}\right) \\ &- \sum_{(\Omega',m')\neq(\Omega_1,m_1)}\mathrm{Re}\left[\Delta^*_{\Omega_1,m_1}\left(\frac{\rho^2_{\Omega',m'(\Omega_1,m_1)}}{\kappa^*_{\Omega',m'(\Omega_1,m_)}} - \kappa_{\Omega',m'(\Omega_1,m_1)}\right)\right] \\ &+ \sum_{(\Omega',m')\neq(\Omega,m)}\mathrm{Re}\left[\Delta^*_{\Omega,m}\left(\frac{\rho^2_{\Omega',m'(\Omega,m)}}{\kappa^*_{\Omega',m'(\Omega,m)}} - \kappa_{\Omega',m'(\Omega,m)}\right)\right]\Bigg\} \end{aligned}$$

$$
\begin{aligned}
&+\frac{\hbar^2}{2J}\Bigg\{\sum_{m'} S_{(\Omega+1,m')(\Omega_1,m_1)}[(I-\Omega)(I+\Omega+1)]^{1/2}\\
&\times\left[\sqrt{\frac{|\kappa_{\Omega,m(\Omega+1,m')}|^2}{\rho_{\Omega,m(\Omega+1,m')}}\frac{|\kappa_{\Omega+1,m'(\Omega,m)}|^2}{\rho_{\Omega+1,m'(\Omega,m)}}}+\kappa^{*}_{\Omega,m(\Omega+1,m')}\kappa_{\Omega+1,m'(\Omega,m)}\sqrt{\frac{\rho_{\Omega,m(\Omega+1,m')}}{|\kappa_{\Omega,m(\Omega+1,m')}|^2}\frac{\rho_{\Omega+1,m'(\Omega,m)}}{|\kappa_{\Omega+1,m'(\Omega,m)}|^2}}\right]\\
&\times\langle\Omega+1,m'|j_+|\Omega,m\rangle T_{\Omega+1,m',\Omega,m}+\sum_{m'} S_{(\Omega-1,m')(\Omega_1,m_1)}[(I+\Omega)(I-\Omega+1)]^{1/2}\\
&\times\left[\sqrt{\frac{|\kappa_{\Omega,m(\Omega-1,m')}|^2}{\rho_{\Omega,m(\Omega-1,m')}}\frac{|\kappa_{\Omega-1,m'(\Omega,m)}|^2}{\rho_{\Omega-1,m'(\Omega,m)}}}+\kappa^{*}_{\Omega,m(\Omega-1,m')}\kappa_{\Omega-1,m'(\Omega,m)}\sqrt{\frac{\rho_{\Omega,m(\Omega-1,m')}}{|\kappa_{\Omega,m(\Omega-1,m')}|^2}\frac{\rho_{\Omega-1,m'(\Omega,m)}}{|\kappa_{\Omega-1,m'(\Omega,m)}|^2}}\right]\\
&\times\langle\Omega-1,m'|j_-|\Omega,m\rangle T_{\Omega-1,m',\Omega,m}\Bigg\}-\frac{\hbar^2}{2J}\Bigg\{\sum_{m'} S_{(\Omega,m)(\Omega_1+1,m')}[(I-\Omega_1)(I+\Omega_1+1)]^{1/2}\\
&\times\left[\sqrt{\frac{|\kappa_{\Omega_1,m_1(\Omega_1+1,m')}|^2}{\rho_{\Omega_1,m_1(\Omega_1+1,m')}}\frac{|\kappa_{\Omega_1+1,m'(\Omega_1,m_1)}|^2}{\rho_{\Omega_1+1,m'(\Omega_1,m_1)}}}+\kappa^{*}_{\Omega_1,m_1(\Omega_1+1,m')}\kappa_{\Omega_1+1,m'(\Omega_1,m_1)}\sqrt{\frac{\rho_{\Omega_1,m_1(\Omega_1+1,m')}}{|\kappa_{\Omega_1,m_1(\Omega_1+1,m')}|^2}\frac{\rho_{\Omega_1+1,m'(\Omega_1,m_1)}}{|\kappa_{\Omega_1+1,m'(\Omega_1,m_1)}|^2}}\right]\\
&\times\langle\Omega_1+1,m'|j_+|\Omega_1,m_1\rangle T_{\Omega_1+1,m',\Omega_1,m}+\sum_{m'} S_{(\Omega,m)(\Omega_1-1,m')}[(I+\Omega_1)(I-\Omega_1+1)]^{1/2}\\
&\times\left[\sqrt{\frac{|\kappa_{\Omega_1,m_1(\Omega_1-1,m')}|^2}{\rho_{\Omega_1,m_1(\Omega_1-1,m')}}\frac{|\kappa_{\Omega_1-1,m'(\Omega_1,m_1)}|^2}{\rho_{\Omega_1-1,m'(\Omega_1,m_1)}}}+\kappa^{*}_{\Omega_1,m_1(\Omega_1-1,m')}\kappa_{\Omega_1-1,m'(\Omega_1,m_1)}\sqrt{\frac{\rho_{\Omega_1,m_1(\Omega_1-1,m')}}{|\kappa_{\Omega_1,m_1(\Omega_1-1,m')}|^2}\frac{\rho_{\Omega_1-1,m'(\Omega_1,m_1)}}{|\kappa_{\Omega_1-1,m'(\Omega_1,m_1)}|^2}}\right]\\
&\times\langle\Omega_1-1,m'|j_-|\Omega_1,m_1\rangle T_{\Omega_1-1,m',\Omega_1,m}\Bigg\}+\sum_{(\Omega',m')\neq(\Omega,m),(\Omega_1,m_1)}^{n} h_{\Omega_1,m_1,m'}S_{(\Omega,m)(\Omega,m')}\\
&-\sum_{(\Omega',m')\neq(\Omega,m),(\Omega_1,m_1)}^{n} h_{\Omega,m',m}S_{(\Omega_1,m')(\Omega_1,m_1)}+h_{\Omega,m_1,m}P_{\Omega,m}-h_{\Omega,m,m_1}P_{\Omega,m_1}. \qquad \text{(A3)}
\end{aligned}
$$

[1] G. Ropke, P. Schuck, Y. Funaki, H. Horiuchi, Z. Ren, A. Tohsaki, C. Xu, T. Yamada, and B. Zhou, Phys. Rev. C **90**, 034304 (2014).
[2] G. Ropke, P. Schuck, C. Xu, Z. Ren, M. Lyu, B. Zhou, Y. Funaki, H. Horiuchi, A. Tohsaki, and T. Yamada, J. Low Temp. Phys. **189**, 383 (2017).
[3] D. Deng, Z. Ren, D. Ni, and Y Qian, J. Phys. G **42**, 075106 (2015).
[4] M. Mirea, Eur. Phys. J. A **51**, 36 (2015).
[5] H. J. Mang, Z. Phys. **148**, 582 (1957).
[6] S. Rosenblum, C. R. Acad. Sci. Paris **188**, 1401 (1929).
[7] E. Segre, *Nuclei and Particles* (Benjamin, New York, 1964), Chap. 7, p. 279.
[8] S. Peltonen, D. S. Delion, and J. Suhonen, Phys. Rev. C **71**, 044315 (2005).
[9] D. S. Delion, in *Theory of Particle and Cluster Emission*, Lecture Notes in Physics Vol. 819 (Springer, Berlin, 2010).
[10] J. O. Rasmussen and B. Segal, Phys. Rev. **103**, 1298 (1956).
[11] A. Sandulescu and M. Iosifescu, Nucl. Phys. **26**, 209 (1961)
[12] D. S. Delion, S. Peltonen, and J. Suhonen, Phys. Rev. C **73**, 014315 (2006).
[13] D. L. Hill and J. A. Wheeler, Phys. Rev. **89**, 1102 (1953).
[14] M. Mirea, Phys. Rev. C **63**, 034603 (2001).
[15] A. Thiel, J. Phys. G **16**, 867 (1990).
[16] J. Y. Park, W. Greiner, and W. Scheid, Phys. Rev. C **21**, 958 (1980).
[17] A. Bohr and B. R. Mottelson, in *Nuclear Structure, Vol. II: Nuclear Deformations* (World Scientific, Singapore, 1998), Appendix 4A, p. 199.
[18] E. Osnes, J. Rekstad, and O. K. Gjotterud, Nucl. Phys. A **253**, 45 (1975).
[19] J. Rekstad, T. Engeland, and E. Osnes, Nucl. Phys. A **330**, 367 (1979).
[20] L. D. Landau, Phys. Z. Sowjet. **2**, 46 (1932).
[21] C. Zener, Proc. R. Soc. A **137**, 696 (1932).
[22] M. Mirea, Mod. Phys. Lett. A **18**, 1809 (2003).
[23] M. Mirea, Phys. Rev. C **78**, 044618 (2008).
[24] W. Greiner, J. Y. Park, and W. Scheid, in *Nuclear Molecules* (World Scientific, Singapore, 1995), Chap. 11.
[25] M. Mirea, Phys. Lett. B **680**, 316 (2009).
[26] M. Mirea, Phys. Rev. C **89**, 034623 (2014).
[27] R. Bernard, H. Goutte, D. Gogny, and W. Younes, Phys. Rev. C **84**, 044308 (2011).
[28] S. E. Koonin and J. R. Nix, Phys. Rev. C **13**, 209 (1976).
[29] J. Blocki and H. Flocard, Nucl. Phys. A **273**, 45 (1976).
[30] B. Avez, C. Simenel, and Ph. Chomaz, Phys. Rev. C **78**, 044318 (2008).

[31] S. Ebata, T. Nakatsukasa, T. Inakura, K. Yoshida, Y. Hashimoto, and K. Yabana, Phys. Rev. C **82**, 034306 (2010).
[32] J. W. Negele, S. E. Koonin, P. Moller, J. R. Nix, and A. J. Sierk, Phys. Rev. C **17**, 1098 (1978).
[33] G. Scamps, C. Simenel, and D. Lacroix, Phys. Rev. C **92**, 011602(R) (2015).
[34] Y. Tanimura, D. Lacroix, and G. Scamps, Phys. Rev. C **92**, 034601 (2015).
[35] M. Mirea, Phys. Rev. C **83**, 054608 (2011).
[36] M. Mirea, Phys. Lett. B **717**, 252 (2012).
[37] D. N. Poenaru and W. Greiner, J. Phys. G **17**, S443 (1991).
[38] A. Zdeb, M. Warda, and K. Pomorski, Phys. Rev. C **87**, 024308 (2013).
[39] H. C. Pauli, Phys. Rep. **7**, 35 (1973).
[40] M. Brack, J. Damgaard, A. Jensen, H. Pauli, V. Strutinsky, and W. Wong, Rev. Mod. Phys. **44**, 320 (1972).
[41] J. R. Nix, Annu. Rev. Nucl. Sci. **22**, 65 (1972).
[42] W. J. Swiatecki and S. Bjornholm, Phys. Rep. **4**, 325 (1972).
[43] T. Lederberger and H. C. Pauli, Nucl. Phys. A **207**, 1 (1973).
[44] M. Mirea, J. Phys. G **43**, 105103 (2016).
[45] D. R. Inglis, Phys. Rev. **96**, 1059 (1954).
[46] D. R. Inglis, Phys. Rev. **97**, 701 (1955).
[47] K. T. R. Davies and J. R. Nix, Phys. Rev. C **14**, 1977 (1976).
[48] P. Moller, J. R. Nix, W. D. Myers, and W. J. Swiatecki, At. Data Nucl. Data Tables **59**, 185 (1995).
[49] V. M. Strutinsky, Nucl. Phys. A **95**, 420 (1967).
[50] S. Cwiok, J. Dudek, W. Nazarewicz, J. Skalski, and Werner, Comput. Phys. Commun. **46**, 379 (1987).
[51] J. Maruhn and W. Greiner, Z. Phys. **251**, 431 (1972).
[52] M. Mirea, Phys. Rev. C **54**, 302 (1996).
[53] M. Mirea, Nucl. Phys. A **780**, 13 (2006).
[54] Y. Aritomo and S. Chiba, Phys. Rev. C **88**, 044614 (2013).
[55] A. Diaz-Torres and W. Scheid, Nucl. Phys. A **757**, 373 (2005).
[56] A. Diaz-Torres, Phys. Rev. Lett. **101**, 122501 (2008).
[57] M. Mirea, R. Budaca, and A. Sandulescu, Ann. Phys. (N.Y.) **380**, 154 (2017).
[58] M. Mirea, D. S. Delion, and A. Sandulescu, Proc. Rom. Acad. Series A **18**, 50 (2017).
[59] A. Sandulescu and M. Mirea, Eur. Phys. J A **50**, 110 (2014).
[60] M. Mirea, D. S. Delion, and A. Sandulescu, Phys. Rev. C **81**, 044317 (2010).
[61] M. Mirea, A. Sandulescu, and D. S. Delion, Nucl. Phys. A **870-871**, 23 (2011).
[62] M. Mirea, A. Sandulescu, and D. S. Delion, Eur. Phys. J. A **48**, 86 (2012).
[63] M. Mirea, Rom. J. Phys. **60**, 156 (2015).
[64] A. Sandulescu, M. Mirea, and D. S. Delion, Europhys. Lett. **101**, 62001 (2013).
[65] D. S. Delion and R. J. Liotta, Phys. Rev. C **87**, 041302(R) (2013).
[66] A. Astier, P. Petkov, M.-G. Porquet, D. S. Delion, and P. Schuck, Eur. Phys. J. A **46**, 165 (2010).
[67] L. J. Jardine, Phys. Rev. C **11**, 1385 (1975).
[68] F. G. Kondev and S. Lalkovski, Nucl. Data Sheets **112**, 707 (2011).
[69] B. Singh *et al.*, Nucl. Data Sheets **114**, 661 (2013).
[70] A. Baran, K. Pomorski, A. Lukasiak, and A. Sobiczewski, Nucl. Phys. A **361**, 83 (1981).
[71] J. A. Wheeler, in *Niels Bohr and the Development of Physics*, edited by W. Pauli, L. Rosenfeld, and W. Weisskopf (Pergamon, London, 1955), p. 163.
[72] R. W. Hasse, Rep. Prog. Phys. **41**, 1027 (1978).
[73] C. Simenel and A. S. Umar, Phys. Rev. C **89**, 031601(R) (2014).
[74] P. Goddard, P. Stevenson, and A. Rios, Phys. Rev. C **93**, 014620 (2016).
[75] A. Bulgac, P. Magierski, K. J. Roche, and I. Stetcu, Phys. Rev. Lett. **116**, 122504 (2016).
[76] N. G. Kelnar, H. M. Castaneda, and M. Nowakowski, Europhys. Lett. **85**, 20006 (2009).
[77] O. Serot, N. Carjan, and D. Strottman, Nucl. Phys. A **569**, 562 (1994).
[78] K. P. Santhosh, J. G. Joseph, and B. Priyanka, Nucl. Phys. A **877**, 1 (2012).
[79] D. N. poenaru, M. Ivascu, and A. Sandulescu, J. Phys. G **5**, L169 (1979).
[80] D. N. Poenaru, D. Schnabel, and W. Greiner, At. Data Nucl. Data Tabl. **48**, 231 (1991).
[81] I. Silisteanu and C. I. Anghel, Rom. J. Phys. **60**, 444 (2015).
[82] C. I. Anghel and I. Silisteanu, Phys. Rev. C **95**, 034611 (2017).
[83] I. Silisteanu and C. I. Anghel, Rom. J. Phys. **62**, 303 (2017).